



## Article

# Mathematical Modeling and Analytical Solution of Thermoelastic Stability Problem of Functionally Graded Nanocomposite Cylinders within Different Theories

Mahmure Avey<sup>1,2,3</sup>, Nicholas Fantuzzi<sup>4,\*</sup>  and Abdullah Sofiyev<sup>2,5,6</sup> 

<sup>1</sup> Department of Mathematical Engineering, Graduate School, Istanbul Technical University, Istanbul 34469, Turkey; mahmureavey@gmail.com or avey22@itu.edu.tr

<sup>2</sup> Information Technology Research and Application Center of Consultancy Board of ITRAC Center, Istanbul Commerce University, Istanbul 34445, Turkey

<sup>3</sup> Analytical Information Resources Center, UNEC-Azerbaijan State Economic University, Baku 1001, Azerbaijan

<sup>4</sup> Department of Civil, Chemical, Environmental, and Materials Engineering, University Bologna, 40126 Bologna, Italy

<sup>5</sup> Department of Civil Engineering, Engineering Faculty, Suleyman Demirel University, Isparta 32260, Turkey; abdullahavey@sdu.edu.tr

<sup>6</sup> Scientific Research Centers for Composition Materials, UNEC-Azerbaijan State Economic University, Baku 1001, Azerbaijan

\* Correspondence: nicholas.fantuzzi@unibo.it

**Abstract:** Revolutionary advances in technology have led to the use of functionally graded nanocomposite structural elements that operate at high temperatures and whose properties depend on position, such as cylindrical shells designed as load-bearing elements. These advances in technology require new mathematical modeling and updated numerical calculations to be performed using improved theories at design time to reliably apply such elements. The main goal of this study is to model, mathematically and within an analytical solution, the thermoelastic stability problem of composite cylinders reinforced by carbon nanotubes (CNTs) under a uniform thermal loading within the shear deformation theory (ST). The influence of transverse shear deformations is considered when forming the fundamental relations of CNT-patterned cylindrical shells and the basic partial differential equations (PDEs) are derived within the modified Donnell-type shell theory. The PDEs are solved by the Galerkin method, and the formula is found for the eigenvalue (critical temperature) of the functionally graded nanocomposite cylindrical shells. The influences of CNT patterns, volume fraction, and geometric parameters on the critical temperature within the ST are estimated by comparing the results within classical theory (CT).

**Keywords:** mathematical modeling; eigenvalue; PDEs; nanocomposites; cylindrical shell; critical temperature

**MSC:** 74G60; 74H55; 74K25; 74F05; 74A40



**Citation:** Avey, M.; Fantuzzi, N.; Sofiyev, A. Mathematical Modeling and Analytical Solution of Thermoelastic Stability Problem of Functionally Graded Nanocomposite Cylinders within Different Theories. *Mathematics* **2022**, *10*, 1081. <https://doi.org/10.3390/math10071081>

Academic Editors: Krzysztof Kamil Żur, Jinseok Kim and J. N. Reddy

Received: 19 February 2022

Accepted: 24 March 2022

Published: 28 March 2022

**Publisher's Note:** MDPI stays neutral with regard to jurisdictional claims in published maps and institutional affiliations.



**Copyright:** © 2022 by the authors. Licensee MDPI, Basel, Switzerland. This article is an open access article distributed under the terms and conditions of the Creative Commons Attribution (CC BY) license (<https://creativecommons.org/licenses/by/4.0/>).

## 1. Introduction

For the development of almost all sectors of the economy, materials with improved performance properties, high strength and light weight, and that are resistant to abrasion, pressure, and various types of radiation are needed. For example, in shipbuilding and civil and mechanical engineering, lightweight and wear-resistant materials are in demand, which are necessary for the creation of structural cladding elements. Developments continue for the aerospace and automotive industries, aiming to reduce the weight and fuel consumption of parts while maintaining the strength of the body and its parts. The nuclear industry needs new materials for power reactors that can withstand high temperatures, pressures, and radiation. In modern technology, the above problems can be solved by using carbon nanotubes or nanocomposites in which they are used as reinforcements. Carbon

nanotubes (CNTs) are carbon allotropes with a cylindrical nanostructure and are classified into single-walled and multi-walled carbon nanotubes. Carbon nanotubes, which have unique electrical, thermal, and mechanical properties with high specific surface areas and aspect ratios, were discovered by Sumio Ijima in 1993 [1]. Depending on their chirality, both their metallic and semiconductor properties made it possible to use CNTs in the field of microelectronics and power engineering, as well as a reinforcing element in the formation of nanocomposites [2–4].

Nanocomposites are generally divided into three categories depending on the type of main matrix: ceramic, metal, and polymer-based nanocomposites. Among these nanocomposite species, polymer nanocomposites are recently in demand. Polymer-based nanocomposites differ from conventional polymer composite materials in lighter weight as well as higher impact and abrasion resistance as well as good resistance to chemical attack, making them suitable for use in military and aerospace developments. The automotive industry is a leader in the growth of the use of nanocomposite materials. Polymer nanocomposites have become the main composite materials for fuel lines, replacing conventional steel to prevent static build-up [5–12]. Today, new results are revealed by performing molecular dynamics (MD) simulations and experimental tests on CNT-reinforced polymers. For example, in the Duan [13] study, based on the hypothesis that only the tube walls in direct contact with the polymer matrix carry the external load, the concept of a true volume ratio for CNT was proposed and a new micromechanical model on the modulus of nanocomposites was developed based on this concept. All these demonstrate that there are still efforts to develop theories about nanocomposites and that interest in this field continues to increase.

With superior performance in very high temperature environments, nanocomposites are among the best new generation composites that can be used as thermal barriers in many advanced technology areas, typically in nuclear reactors, spacecraft, and aerospace. As cylindrical shell structures are one of the main structural elements made up of nanocomposites, perhaps the first, there is a further need to investigate their buckling behavior in the thermal environment and under thermal loading. After the first attempt by Shen [14] on thermal buckling of nanocomposite cylindrical shells, some research has been done on this topic [15–38]. Most of these studies are related to the buckling problem of FG-CNT-reinforced structural elements in the thermal environment or thermal loading, and their solutions have been realized by using various theories and numerical methods.

The literature review revealed that the investigation of the thermal stability behavior of cylindrical shells based on CNTs is insufficient. In this study, the analytical solution of the thermal stability problem of composite cylinders reinforced by CNTs under the uniform thermal loading is presented within different theories. This study will be beneficial in terms of updating the buckling analysis of cylindrical shells made of carbon nanotube-reinforced composites in the thermal environment and developing calculation methods during the design. As one of the main structural elements consisting of nanocomposites is the cylindrical shell, examining the buckling behavior in the thermal environment and under thermal loading will help to eliminate the problems that may arise in industries where advanced technologies are used during the design phase. The analytical solution of the buckling problem of cylindrical shells made of nanocomposites within the framework of various theories in the thermal environment and obtaining original formulas is also an important achievement from a mathematical point of view.

## 2. Material Methods

### 2.1. Theoretical Development

Consider the CNT-reinforced composite cylindrical shell of radius  $a$ , length  $l$ , and thickness  $h$  under the uniform thermal loading. The  $Oxyz$  coordinate system is located at the left end of the mid-surface of the cylinder, and the  $x, y, z$  axes are oriented, as in Figure 1.

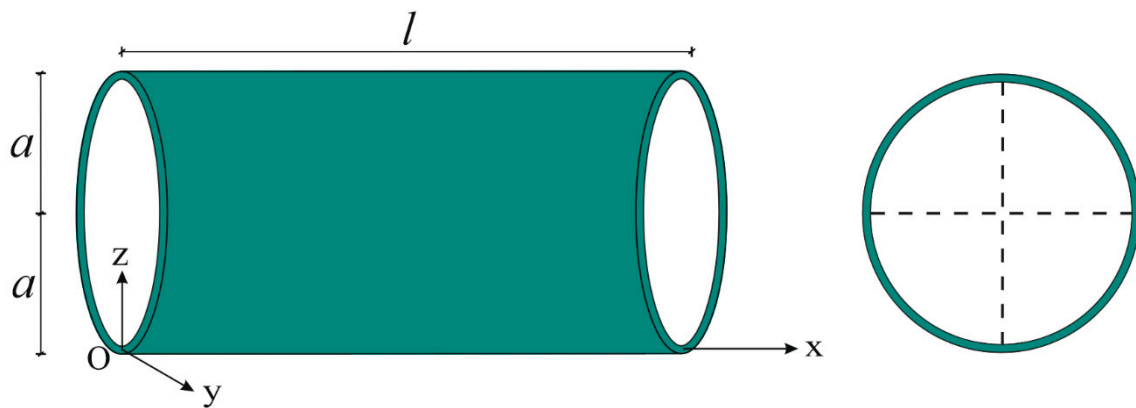


Figure 1. CNT-reinforced composite cylindrical shell and coordinate system.

Three common approaches are used for the modeling of carbon nanotube-reinforced composites: (1) atomistic modeling, e.g., molecular dynamics (MD) simulations; (2) continuum mechanics modeling; and (3) multiscale modeling. Besides atomic modeling, continuum mechanics (or micromechanical models) has been extended to modeling of the mechanical properties of nanocomposites. Among the micromechanical models, the most popular are the rule of mixture (RM), the Mori-Tanaka (MT) model, and the representative volume element (RVE) model. In this study, the effective material properties, such as Young’s modulus and Poisson’s ratio of nanocomposite cylindrical shells, are obtained using the RM method and are expressed as follows [14,17,35]:

$$\begin{aligned}
 Y_{11}(\bar{z}) &= \eta_1 V_{cnt}(\bar{z}) Y_{11}^{cnt} + V^m Y^m, \quad \frac{\eta_2}{Y_{22}(\bar{z})} = \frac{V_{cnt}(\bar{z})}{Y_{22}^{cnt}} + \frac{V^m}{Y^m}, \quad \frac{\eta_3}{G_{12}(\bar{z})} = \frac{V_{cnt}(\bar{z})}{G_{12}^{cnt}} + \frac{V^m}{G^m}, \quad G_{13}(\bar{z}) = G_{12}(\bar{z}), \\
 G_{23}(\bar{z}) &= 1.2 G_{12}(\bar{z}), \quad \nu_{12} = V_{cnt}^* \nu_{12}^{cnt} + V^m \nu^m, \quad \rho = V_{cnt}^* \rho^{cnt} + V^m \rho^m, \quad V_{cnt}(\bar{z}) + V_m = 1
 \end{aligned}
 \tag{1}$$

where  $V$  denotes the volume fraction, superscript “ $cnt$ ” and “ $m$ ” represent the corresponding property for CNT and matrix, respectively, the efficiency parameters are indicated by  $\eta_i$  ( $i = 1, 2, 3$ ), and the Young and shear moduli of the polymer (or matrix) and CNTs are indicated by  $Y^m, Y_{kk}^{cnt}$  ( $k = 1, 2$ ) and  $G_{12}^{cnt}$ , respectively. Here  $\nu_{12}$  and  $\rho$  are Poisson’s ratio and density, respectively.

The volume fraction of the CNTs changes as a linear function depending on the dimensionless thickness coordinate ( $\bar{z} = z/h$ ) of the cylindrical shell [14–19].

$$V_{cnt}(\bar{z}) = \begin{cases} U & \text{at } V_{cnt}^* \\ V & \text{at } (1 - 2\bar{z})V_{cnt}^* \\ O & \text{at } (1 + 2\bar{z})V_{cnt}^* \\ X & \text{at } 4|\bar{z}|V_{cnt}^* \end{cases}
 \tag{2}$$

where

$$V_{cnt}^* = \frac{m_{cnt}}{m_{cnt} \left(1 - \frac{\rho_{cnt}}{\rho_m}\right) + \frac{\rho_{cnt}}{\rho_m}}
 \tag{3}$$

in which  $m_{cnt}$  is a mass fraction of CNTs.

The use of these relations is based on the following hypotheses: CNTs are reinforced into the polymer matrix as linear functions and CNTs reinforced into the polymer matrix carry the charge transferred to the matrix.

While the first line of the Equation (2) shows that the CNT distribution is uniform (U), the other distributions are in the form of linear functions and are represented by the symbols V, O, and X, respectively. Based on Equation (2), the patterns formed by the CNT distribution throughout the thickness of the polymer cylindrical shell are illustrated in Figure 2.

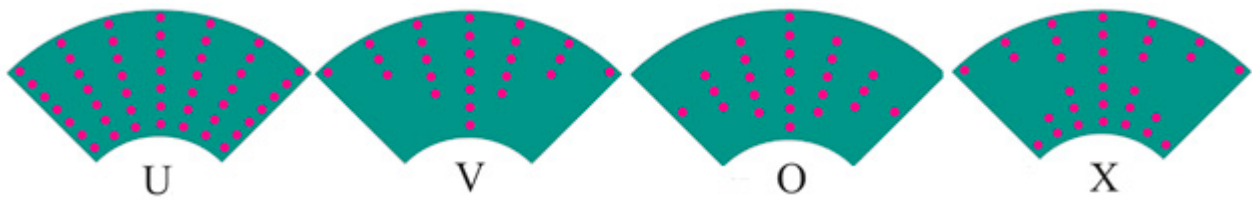


Figure 2. CNT distribution throughout the thickness of the polymer cylindrical shell.

In this study, it is assumed that the thermal expansion coefficients, as well as the material properties, vary with temperature and location [14,16,17,34]:

$$\alpha_{11}(\bar{z}) = \frac{\alpha_{11}^{cnt} V_{cnt}(\bar{z}) Y_{11}^{cnt} + V^m \gamma^m \alpha^m}{V_{cnt}(\bar{z}) Y_{11}^{cnt} + V^m \gamma^m}, \quad \alpha_{22}(\bar{z}) = (1 + \nu_{12}^{cnt}) \alpha_{22}^{cnt} V_{cnt}(\bar{z}) + (1 + \nu^m) V^m \alpha^m - \nu_{12} \alpha_{11}(\bar{z}) \tag{4}$$

where  $\alpha_{11}^{cnt}$ ,  $\alpha_{22}^{cnt}$ , and  $\alpha^m$  are thermal expansion coefficients of CNT and matrix, respectively.

2.2. Governing Equations

If we generalize the ST to the heterogeneous nanocomposite cylindrical shells, the displacement components can be represented as follows [34,37–39]

$$u_1(x, y, z) = u(x, y) + z\varphi_1(x, y), \quad v_1(x, y, z) = v(x, y) + z\varphi_2(x, y), \quad w_1(x, y, z) = w(x, y) \tag{5}$$

where  $u$  and  $v$  are the displacements of axial and circumferential directions on the reference surface, respectively,  $w$  is the deflection, and  $\varphi_1(x, y)$  and  $\varphi_2(x, y)$  are the transverse normal rotations about the  $y$  and  $x$  axes, respectively.

Considering the assumptions of the ST [39], the following relations can be written:

$$e_{33} = 0, \quad \sigma_{13} = \frac{df_1}{dz} \varphi_1(x, y), \quad \sigma_{23} = \frac{df_2}{dz} \varphi_2(x, y) \tag{6}$$

where  $e_{33}$  is the normal strain in the direction  $z$ ,  $\sigma_{i3}$  ( $i = 1, 2$ ) are the transverse shear stresses, and  $f_i(z)$ , ( $i = 1, 2$ ) are the shape functions of transverse shear deformations (TSDs) of the CNT-originated cylindrical shells [37–39].

The basic relationships of CNT-originated cylindrical shells under the temperature field are constructed in the scope of ST as follows [14,17,34,35,40]:

$$\begin{bmatrix} \sigma_{11} \\ \sigma_{22} \\ \sigma_{12} \\ \sigma_{13} \\ \sigma_{23} \end{bmatrix} = \begin{bmatrix} A_{11}(\bar{z}) & A_{12}(\bar{z}) & 0 & 0 & 0 \\ A_{21}(\bar{z}) & A_{22}(\bar{z}) & 0 & 0 & 0 \\ 0 & 0 & A_{66}(\bar{z}) & 0 & 0 \\ 0 & 0 & 0 & A_{55}(\bar{z}) & 0 \\ 0 & 0 & 0 & 0 & A_{44}(\bar{z}) \end{bmatrix} \begin{bmatrix} e_{11} \\ e_{22} \\ \gamma_{12} \\ \gamma_{13} \\ \gamma_{23} \end{bmatrix} + \begin{bmatrix} \sigma_{1T} \\ \sigma_{2T} \\ 0 \\ 0 \\ 0 \end{bmatrix} \tag{7}$$

where  $\sigma_{ij}$  ( $i = 1, 2, j = 1, 2, 3$ ) and  $e_{ii}$  ( $i = 1, 2$ ),  $\gamma_{ij}$  ( $i = 1, 2, j = 2, 3$ ) indicate stresses and strains, respectively, and  $A_{ij}$  ( $i, j = 1, 2, \dots, 6$ ) are given as:

$$A_{11}(\bar{z}) = \frac{Y_{11}(\bar{z})}{1 - \nu_{12}\nu_{21}}, \quad A_{12}(\bar{z}) = \frac{\nu_{21}Y_{11}(\bar{z})}{1 - \nu_{12}\nu_{21}}, \quad A_{21}(\bar{z}) = \frac{\nu_{12}Y_{22}(\bar{z})}{1 - \nu_{12}\nu_{21}}, \quad A_{22}(\bar{z}) = \frac{Y_{22}(\bar{z})}{1 - \nu_{12}\nu_{21}} \tag{8}$$

$$A_{44}(\bar{z}) = G_{23}(\bar{z}) = 2G_{12}(\bar{z}), \quad A_{55}(\bar{z}) = G_{13}(\bar{z}) = G_{12}(\bar{z}), \quad A_{66}(\bar{z}) = G_{12}(\bar{z})$$

in which  $\sigma_{1T}$  and  $\sigma_{2T}$  are defined by

$$\sigma_{1T} = -\frac{Y_{11}(\bar{z})\alpha_{11}(\bar{z})T(\bar{z})}{1 - \nu_{12}\nu_{21}}, \quad \sigma_{2T} = -\frac{Y_{22}(\bar{z})\alpha_{22}(\bar{z})T(\bar{z})}{1 - \nu_{12}\nu_{21}} \tag{9}$$

By using the Equations (6) and (7), the components of the strain field ( $e_{11}, e_{22}, \gamma_{12}$ ) at an arbitrary point of CNT-originated shells can be expressed as those of its mid-surface ( $e_{011}, e_{022}, \gamma_{012}$ ) and its curvature changes as follows:

$$\begin{bmatrix} e_{11} \\ e_{22} \\ \gamma_{12} \end{bmatrix} = \begin{bmatrix} e_{011} - z \frac{\partial^2 w}{\partial x^2} + I_1(z) \frac{\partial \varphi_1}{\partial x} \\ e_{022} - z \frac{\partial^2 w}{\partial y^2} + I_2(z) \frac{\partial \varphi_2}{\partial y} \\ \gamma_{012} - 2z \frac{\partial^2 w}{\partial x \partial y} + I_1(z) \frac{\partial \varphi_1}{\partial y} + I_2(z) \frac{\partial \varphi_2}{\partial x} \end{bmatrix} \tag{10}$$

where

$$I_1(z) = \int_0^z \frac{df_1}{dz} \frac{1}{G_{13}(\bar{z})} dz, \quad I_2(z) = \int_0^z \frac{df_2}{dz} \frac{1}{G_{23}(\bar{z})} dz \tag{11}$$

The in-plane forces ( $N_{ij}$  ( $i, j = 1, 2$ )), transverse shear forces ( $Q_i$  ( $i = 1, 2$ )), and the bending and twisting moments ( $M_{ij}$  ( $i, j = 1, 2$ )) per unit length are found as follows [37–39]:

$$(N_{ij}, Q_i, M_{ij}) = \int_{-0.5h}^{0.5h} (\sigma_{ij}, \sigma_{i3}, \sigma_{ijz}) dz \tag{12}$$

We can also find the thermal forces and moments ( $N_{11}^T, N_{22}^T, M_{11}^T, M_{22}^T$ ) using the following integrals [14,17,34,37,41]:

$$\begin{bmatrix} N_{11}^T, M_{11}^T \\ N_{22}^T, M_{22}^T \end{bmatrix} = \int_{-h/2}^{h/2} \begin{bmatrix} A_{11}(\bar{z}), A_{12}(\bar{z}) \\ A_{21}(\bar{z}), A_{22}(\bar{z}) \end{bmatrix} \begin{bmatrix} \alpha_{11} \\ \alpha_{22} \end{bmatrix} (1, z) \Delta T dz \tag{13}$$

In the cylinder, when the temperature rises evenly, the temperature gradually increases from the first value to the last value, while the temperature difference  $\Delta T = T - T_0$  remains constant.

The relationship between stress function ( $F$ ) and force components is as follows [37–39]:

$$N_{11} = h \frac{\partial^2 F}{\partial y^2}, \quad N_{12} = -h \frac{\partial^2 F}{\partial x \partial y}, \quad N_{22} = h \frac{\partial^2 F}{\partial x^2} \tag{14}$$

The membrane form of the equilibrium equations can be written as [14,17,34,35]:

$$N_{11}^0 = -\tilde{N} = - \int_{-h/2}^{h/2} [A_{11}(\bar{z})\alpha_{11}(\bar{z}) + A_{12}(\bar{z})\alpha_{22}(\bar{z})] \Delta T dz, \quad N_{22}^0 = 0, \quad N_{12}^0 = 0 \tag{15}$$

where  $N_{11}^0$  and  $\tilde{N}$  are the pre-buckling thermal force and thermal parameter.

Substituting the forces, moments, and strains on the middle surface, expressed as  $w, F, \varphi_1, \varphi_2$ , using relations (7), (10), and (12)–(14) into the governing equations [37–39]: one gets:

$$\begin{aligned} & h(c_{11} - c_{31}) \frac{\partial^4 F}{\partial x^2 \partial y^2} + hc_{12} \frac{\partial^4 F}{\partial x^4} - c_{13} \frac{\partial^4 w}{\partial x^4} - (c_{14} + c_{32}) \frac{\partial^4 w}{\partial x^2 \partial y^2} + c_{15} \frac{\partial^3 \varphi_1}{\partial x^3} + c_{35} \frac{\partial^3 \varphi_1}{\partial x \partial y^2} \\ & - I_3 \frac{\partial \varphi_1}{\partial x} c_{18} \frac{\partial^3 \varphi_2}{\partial x^2 \partial y} + c_{38} \frac{\partial^3 \varphi_2}{\partial x^2 \partial y} = 0, \\ & hc_{21} \frac{\partial^4 F}{\partial y^4} + h(c_{22} - c_{31}) \frac{\partial^4 F}{\partial x^2 \partial y^2} - (c_{32} + c_{23}) \frac{\partial^4 w}{\partial x^2 \partial y^2} - c_{24} \frac{\partial^4 w}{\partial y^4} + c_{35} \frac{\partial^3 \varphi_1}{\partial x \partial y^2} + c_{25} \frac{\partial^3 \varphi_1}{\partial x \partial y^2} \\ & + c_{38} \frac{\partial^3 \varphi_2}{\partial x^2 \partial y} + c_{28} \frac{\partial^3 \varphi_2}{\partial y^3} - I_4 \frac{\partial \varphi_2}{\partial y} = 0 \tag{16} \\ & hb_{11} \frac{\partial^4 F}{\partial y^4} + h(b_{12} + b_{21} + b_{31}) \frac{\partial^4 F}{\partial x^2 \partial y^2} + hb_{22} \frac{\partial^4 F}{\partial x^4} - b_{23} \frac{\partial^4 w}{\partial x^4} - (b_{24} + b_{13} - b_{32}) \frac{\partial^4 w}{\partial x^2 \partial y^2} - b_{14} \frac{\partial^4 w}{\partial y^4} \\ & + \frac{1}{a} \frac{\partial^2 w}{\partial x^2} + b_{25} \frac{\partial^3 \varphi_1}{\partial x^3} + b_{15} \frac{\partial^3 \varphi_1}{\partial x \partial y^2} + b_{35} \frac{\partial^3 \varphi_1}{\partial x \partial y^2} + b_{28} \frac{\partial^3 \varphi_2}{\partial x^2 \partial y} + b_{38} \frac{\partial^3 \varphi_2}{\partial x^2 \partial y} + b_{18} \frac{\partial^3 \varphi_2}{\partial y^3} = 0, \\ & \frac{h}{a} \frac{\partial^2 F}{\partial x^2} + N_{11}^0 \frac{\partial^2 w}{\partial x^2} + I_3 \frac{\partial \varphi_1}{\partial x} + I_4 \frac{\partial \varphi_2}{\partial y} = 0. \end{aligned}$$

where  $b_{ij}$  and  $c_{ij}$  ( $i = 1, 2, 3; j = 1, 2, \dots, 8$ ) are described in Appendix A.

### 2.3. Solution Method

The CNT-reinforced nanocomposite cylindrical shell is subject to simply supported boundary conditions at the edges and is mathematically expressed as [39]:

$$w = 0, \quad M_{11} = 0, \quad \varphi_2 = 0, \quad \frac{\partial^2 F}{\partial y^2} = 0 \text{ when } x = 0, \quad x = l \quad (17)$$

The solution of the set of Equation (16), which satisfies the above boundary conditions, is sought as follows [35,39]:

$$\begin{aligned} w &= \Lambda_1 \sin(\lambda x) \sin(\mu y), \quad F = \Lambda_2 \sin(\lambda x) \sin(\mu y), \\ \varphi_1 &= \Lambda_3 \cos(\lambda x) \sin(\mu y), \quad \varphi_2 = \Lambda_4 \sin(\lambda x) \cos(\mu y) \end{aligned} \quad (18)$$

where  $\Lambda_i (i = 1, 2, \dots, 4)$  are unknown amplitudes,  $(\lambda, \mu) = (m\pi l^{-1}, n a^{-1})$ , in which  $(m, n)$  is the buckling mode.

To find the expression for the critical temperature, expressions (18) are substituted into the basic Equations (16) and after applying the Galerkin method, the determinant of the matrix of coefficients of algebraic equations is equal to zero:

$$p_{41}D_1 - \tilde{N}\lambda^2 D_2 + p_{43}D_3 + p_{44}D_4 = 0 \quad (19)$$

where

$$D_1 = - \begin{vmatrix} p_{12} & p_{13} & p_{14} \\ p_{22} & p_{23} & p_{24} \\ p_{32} & p_{33} & p_{34} \end{vmatrix}, \quad D_2 = \begin{vmatrix} p_{11} & p_{13} & p_{14} \\ p_{21} & p_{23} & p_{24} \\ p_{31} & p_{33} & p_{34} \end{vmatrix}, \quad D_3 = - \begin{vmatrix} p_{11} & p_{12} & p_{14} \\ p_{21} & p_{22} & p_{24} \\ p_{31} & p_{32} & p_{34} \end{vmatrix}, \quad D_4 = \begin{vmatrix} p_{11} & p_{12} & p_{13} \\ p_{21} & p_{22} & p_{23} \\ p_{31} & p_{32} & p_{33} \end{vmatrix} \quad (20)$$

in which

$$\begin{aligned} p_{11} &= [(c_{11} - c_{31})\lambda^2\mu^2 + c_{12}\lambda^4]h, \quad p_{12} = (c_{14} + c_{32})\lambda^2\mu^2 + c_{13}\lambda^4, \quad p_{13} = c_{15}\lambda^3 + c_{35}\lambda\mu^2 + I_3\lambda, \\ p_{14} &= (c_{18} + c_{38})\mu\lambda^2, \quad p_{21} = [c_{21}\mu^4 + (c_{22} - c_{31})\lambda^2\mu^2]h, \quad p_{22} = (c_{32} + c_{23})\lambda^2\mu^2 + c_{24}\mu^4, \\ p_{23} &= (c_{25} + c_{35})\lambda\mu^2, \quad p_{24} = c_{28}\mu^3 + c_{38}\lambda^2\mu + I_4\mu, \quad p_{31} = h[b_{22}\lambda^4 + (b_{12} + b_{21} + b_{31})\lambda^2\mu^2 + b_{11}\mu^4], \\ p_{32} &= b_{23}\lambda^4 + (b_{24} + b_{13} + b_{32})\lambda^2\mu^2 + b_{14}\mu^4 + \lambda^2/a, \quad p_{33} = b_{25}\lambda^3 + (b_{15} + b_{35})\lambda\mu^2, \\ p_{34} &= (b_{28} + b_{38})\lambda^2\mu + b_{18}\mu^3, \quad p_{41} = \lambda^2h/a, \quad p_{43} = I_3\lambda, \quad p_{44} = I_4\mu \end{aligned} \quad (21)$$

To find the eigenvalue or the critical uniform temperature (CUT) for the CNT patterned cylinders within ST, Equations (15) and (19) are solved together and the following closed form solution is obtained:

$$T_{sdt}^{cr} = \frac{p_{41}D_1 + p_{43}D_3 + p_{44}D_4}{\eta D_2 \lambda^2} \quad (22)$$

where

$$\eta = \int_{-h/2}^{h/2} [A_{11}(\bar{z})\alpha_{11}(\bar{z}) + A_{12}(\bar{z})\alpha_{22}(\bar{z})] dz \quad (23)$$

When TSDs are ignored in the basic relationships, the expression (24) transforms into the expression for CUT of the nanocomposite cylindrical shells within CT and it is shown as  $T_{cst}^{cr}$ .

The critical uniform temperature of nanocomposite cylindrical shells within the ST is found by minimizing Equation (22) versus the  $(m, n)$ .

### 3. Results

In this section, to confirm the accuracy of the analytical solution obtained in this study, first a comparison is made with an existing and reliable result, and then original analyses are performed.



### 3.1. Comparative Study

In this subsection, the results for the buckling load of cylindrical shells modeled with different types of CNTs in a thermal environment and under axial load are compared with solutions of ref. [41] within ST and given in Table 1. As Shen [41] used  $N_{shen}^{cr} = 2\pi a N_{sdt}^{cr}$ , we use the formula (22) by multiplying  $2\pi a$  at  $N_{11}^0 = -N$ , where  $N$  is the uniform axial load. The nanocomposite cylindrical shell characteristics are:  $a/h = 30$ ,  $h = 0.002$  m,  $V_{cnt}^* = 0.17$ ,  $l = 10\sqrt{3ah}$  [41]. It is observed from Table 1 that current results for  $N_{shen}^{cr} = 2\pi a N_{sdt}^{cr}$  (in kN) of the cylinder with U and X profiles are in good agreement with the results of ref. [41] in the thermal environment.

**Table 1.** Comparison of critical axial load of cylinders reinforced with U- and X-model in the thermal environment within ST.

$N_{shen}^{cr} = 2\pi a N_{sdt}^{cr} (m,n)$			
U	X	U	X
Ref. [41]		Current study	
122.25	148.06	122.440 (2,4)	148.966 (1,3)

### 3.2. Analysis and Interpretations

The thermomechanical properties of PMMA and CNT at room temperature, that is, for  $T = 300$  K, are numerically obtained using the following temperature-dependent functions. [14,17]:

$$\begin{aligned}
 Y^m &= (3.52 - 0.0034T) = 2.5 \text{ GPa}, \quad \alpha^m = 45(1 + 0.0005\Delta T) \times 10^{-6} = 45 \times 10^{-6} / \text{K}, \quad \nu^m = 0.34, \\
 Y_{11}^{cnt} &= (6.18387 - 2.86 \times 10^{(-3)} \times T + 4.22867 \times 10^{(-6)} \times T^2 - 2.2724 \times 10^{(-9)} \times T^3) = 5.6451 \text{TPa} \\
 Y_{22}^{cnt} &= (7.75348 - 3.58 \times 10^{(-3)} \times T + 5.30057 \times 10^{(-6)} \times T^2 - 2.84868 \times 10^{(-9)} \times T^3) = 7.0796 \text{TPa} \\
 G_{12}^{cnt} &= (1.80126 + 0.77845 \times 10^{(-3)} \times T - 1.1279 \times 10^{(-6)} \times T^2 + 4.93484 \times 10^{(-10)} \times T^3) = 1.9466 \text{TPa} \\
 \alpha_{11}^{cnt} &= (-1.12148 + 2.289 \times 10^{(-2)} \times T - 2.88155 \times 10^{(-5)} \times T^2 + 1.13253 \times 10^{(-8)} \times T^3) \times 10^{(-6)} = 3.4579 \times 10^{(-6)} / \text{K} \\
 \alpha_{22}^{cnt} &= (5.43874 - 9.95498 \times 10^{(-4)} \times T + 3.13525 \times 10^{(-7)} \times T^2 - 3.56332 \times 10^{(-12)} \times T^3) \times 10^{(-6)} = 5.1682 \times 10^{(-6)} / \text{K}
 \end{aligned}$$

The efficiency parameters are described by [41]:

$$\begin{aligned}
 \eta_1 &= 0.137, \quad \eta_2 = 1.022, \quad \eta_3 = 0.7\eta_2 \quad \text{at} \quad V_{cnt}^* = 0.12; \quad \eta_1 = 0.142, \quad \eta_2 = 1.626, \quad \eta_3 = 0.7\eta_2 \quad \text{at} \quad V_{cnt}^* = 0.17; \\
 \eta_1 &= 0.141, \quad \eta_2 = 1.585, \quad \eta_3 = 0.7\eta_2 \quad \text{at} \quad V_{cnt}^* = 0.28
 \end{aligned}$$

The CNT sizes are as follows:  $l_{cnt} = 9.26$  nm,  $a_{cnt} = 0.68$  nm,  $h_{cnt} = 0.067$  nm,  $\nu_{12}^{cnt} = 0.175$ , and  $f_1(z) = f_2(z) = z - \frac{4}{3h^2}z^3$  [39–41].

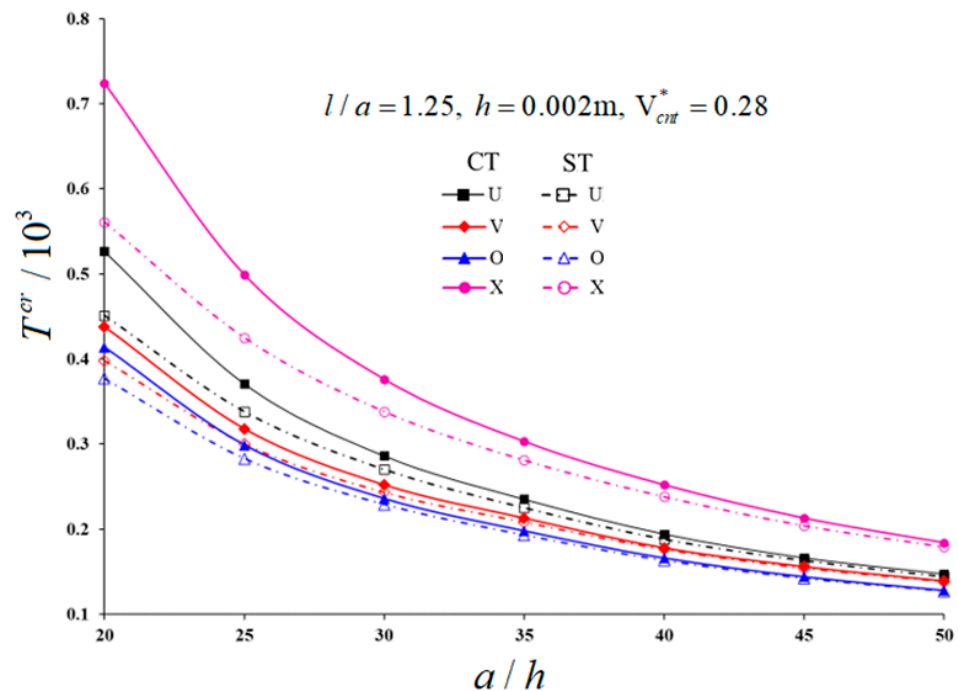
Table 2 presents the variation of the critical uniform temperature when the CNT cylindrical shell parameters are  $l/a = 1.25$ ,  $h/a = 0.05$ ,  $h = 0.002$  m. It was determined that the critical temperature values decrease significantly, while those change irregularly, as the volume fraction increases. In addition, although the critical temperature decreases significantly, the number of waves corresponding to the minimum critical temperature does not change. The highest influence of TSDs on CUT is 22.51%, occurring in the X-pattern at  $V_{cnt}^* = 0.28$ , while the smallest effect is 6.01%, occurring in the O-model at  $V_{cnt}^* = 0.17$ . V-, O-, and X-patterns exhibit different effects compared to the U-model. In the framework of ST, the largest pattern effect on the critical temperature occurs in the X-model (+24.39%) for  $V_{cnt}^* = 0.28$ , whereas the least influence occurs in the V-model (−10.16%) for  $V_{cnt}^* = 0.17$ . It is observed that the pattern effect on the CUT value in the framework of CT is more pronounced than ST, between 11% and 13% in the X-pattern, between 3% and 4% in the O-pattern, and between 3% and 5% in the V-pattern. In addition, among these patterns, only the critical temperature values in the X-pattern are greater than the values in the U-pattern, and therefore the (+) sign is placed in front of them.

Figure 3 shows the changes of the critical uniform temperature depending on the  $a/h$  ratio within ST and CT when the CNT cylinder parameters are  $l/a = 1.25$ ,  $h = 0.002$  m,  $V_{cnt}^* = 0.28$ . It is observed that the magnitudes of the critical temperature continuously reduce with the increase in the  $a/h$  ratio. The influences of TSDs on the critical temperature decrease with

the increasing of the ratio,  $a/h$ . The influences of TSDs on the critical temperature for the U-, V-, O-, and X-patterns are 14.42%, 9.13%, 8.94%, and 22.51%, respectively, as  $a/h = 20$ , while those effects are 2.04%, 0.72%, 0.78%, and 2.72%, respectively, as  $a/h = 50$  (Figure 3). For some models, when  $a/h > 50$ , CT can be used instead of ST. When compared with the uniform pattern, the effects of the V- and O- patterns on the CUT decrease from (−11.75%) to (−4.17%) and from (−16.41%) to (−11.81%), respectively, with the increase in  $a/h$  from 20 to 50, while this effect changes irregularly in the X-model, around 24.4–26.6%. In addition, it is observed that the consideration of transverse shear deformations significantly reduces the effect of patterns on critical temperatures.

**Table 2.** Variation of CUT for nanocomposite cylindrical shells with different volume fractions.

$V_{cnt}^*$	$T^{cr}/10^3(K)$							
	U		V		O		X	
	CT	ST	CT	ST	CT	ST	CT	ST
0.12	0.533 (1,4)	0.472 (1,4)	0.455 (1,4)	0.420 (1,4)	0.415 (1,4)	0.385 (1,4)	0.695 (1,4)	0.574 (1,4)
0.17	0.568 (1,4)	0.512 (1,4)	0.492 (1,4)	0.460 (1,4)	0.449 (1,4)	0.422 (1,4)	0.738 (1,4)	0.625 (1,4)
0.28	0.527 (1,4)	0.451 (1,4)	0.438 (1,4)	0.398 (1,4)	0.414 (1,4)	0.377 (1,4)	0.724 (1,4)	0.561 (1,4)



**Figure 3.** Variation of CUT for nanocomposite cylindrical shells against the  $a/h$  ratio within ST and CT.

Figure 4 shows the variation of the CUT depending on the  $l/a$  ratio within different theories, as the CNT cylindrical shell characteristics are  $h/a = 0.05$ ,  $h = 0.002$  m, and  $V_{cnt}^* = 0.28$ . As can be observed, CUT values decrease continuously depending on the  $l/a$  ratio, and this decrease is evident. The fastest decrease is observed in the U- and X- patterned cylindrical shell in the framework of ST. The use of the shear deformation theory significantly reduces the critical temperature values compared to the CT. The shear deformations effect on the CUT demonstrates that it decreases with the increase in  $l/a$ . For example, at  $l/a = 0.75$ , the effects of TSDs on the CUT are 36.96%, 26.51%, 26.44%, and 49.3% for the U-, V-, O-, and X-patterns, respectively, while those effects are 2.02%, 1.44%, 0.94%, and 3.56%, respectively, as  $l/a = 2.5$ . Although CT can be used instead of ST for  $l/a > 2$  ratios in some patterns, its use at high temperatures may lead to incorrect results. When compared with the uniform pattern, the influences of the V- and O-patterns on the



CUT reduce from (−15.09%) to (0.588%) and (−16.4%) and (−7.06%), respectively, with the increase in  $l/a$  from 0.75 to 2.25, while this effect changes irregularly in the X-model, at around 16.26–24.4%. As can be observed from the calculations, using CT does not cause an error when  $l \geq 2.5a$  in V-patterned cylindrical shells.

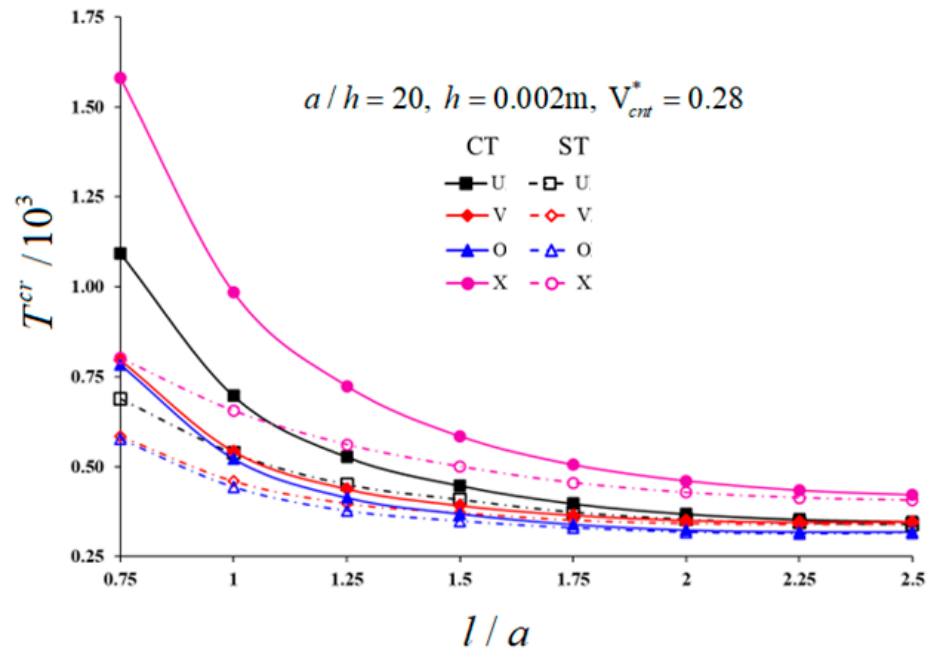


Figure 4. Variation of CUT against the  $l/a$  ratio within ST and CT.

#### 4. Conclusions

In this study, thermal buckling behaviors of nanocomposite cylindrical shells are discussed in the scope of the ST. The basic relations of CNT-patterned cylindrical shells are first constructed, and then the governing equations are derived within the framework of the modified Donnell-type shell theory, considering the effect of TSDs. By solving the basic PDEs with the Galerkin method, the closed-form solution for the CUT of nanocomposite cylindrical shells is found. The effects of CNT patterns, volume fraction, and cylinder parameters on the critical uniform temperature within the ST are estimated in comparison with the results in the framework of the CT.

**Author Contributions:** Conceptualization, M.A.; methodology, M.A.; software, M.A. and N.F.; validation, M.A. and N.F.; formal analysis, M.A.; investigation, M.A.; resources, M.A.; data curation, M.A.; writing—original draft preparation, M.A.; writing—review and editing, M.A., N.F. and A.S.; visualization, M.A.; supervision, M.A. All authors have read and agreed to the published version of the manuscript.

**Funding:** This research received no external funding.

**Institutional Review Board Statement:** Not applicable.

**Informed Consent Statement:** Not applicable.

**Data Availability Statement:** Not applicable.

**Conflicts of Interest:** The authors declare no conflict of interest.

### Appendix A

In Equation (16), the following definitions apply:

$$\begin{aligned}
 c_{11} &= a_{11}^1 b_{11} + a_{12}^1 b_{21}, & c_{12} &= a_{11}^1 b_{12} + a_{12}^1 b_{22}, & c_{13} &= a_{11}^1 b_{13} + a_{12}^1 b_{23} + a_{21}^2 \\
 c_{14} &= a_{11}^1 b_{14} + a_{12}^1 b_{24} + a_{12}^2, & c_{15} &= a_{11}^1 b_{15} + a_{12}^1 b_{25} + a_{15}^1, & c_{18} &= a_{11}^1 b_{18} + a_{12}^1 b_{28} + a_{18}^1, \\
 c_{21} &= a_{21}^1 b_{11} + a_{22}^1 b_{21}, & c_{22} &= a_{21}^1 b_{12} + a_{22}^1 b_{22}, & c_{23} &= a_{21}^1 b_{13} + a_{22}^1 b_{23} + a_{21}^2, \\
 c_{24} &= a_{21}^1 b_{14} + a_{22}^1 b_{24} + a_{22}^2, & c_{25} &= a_{21}^1 b_{15} + a_{22}^1 b_{25} + a_{25}^1, & c_{28} &= a_{21}^1 b_{18} + a_{22}^1 b_{28} + a_{28}^1, \\
 c_{31} &= a_{66}^1 b_{31}, & c_{32} &= a_{66}^1 b_{32} + 2a_{66}^2, & c_{35} &= a_{35}^1 - a_{66}^1 b_{35}, & c_{38} &= a_{38}^1 - a_{66}^1 b_{38}, \\
 b_{11} &= \frac{a_{22}^0}{d}, & b_{12} &= -\frac{a_{12}^0}{d}, & b_{13} &= \frac{a_{12}^0 a_{21}^1 - a_{11}^1 a_{22}^0}{d}, & b_{14} &= \frac{a_{12}^0 a_{22}^1 - a_{12}^1 a_{22}^0}{d}, \\
 b_{15} &= \frac{a_{25}^0 a_{12}^0 - a_{15}^0 a_{22}^0}{d}, & b_{18} &= \frac{a_{28}^0 a_{12}^0 - a_{18}^0 a_{22}^0}{d}, & b_{21} &= -\frac{a_{21}^0}{d}, & b_{22} &= \frac{a_{11}^0}{d}, \\
 b_{23} &= \frac{a_{11}^1 a_{21}^0 - a_{21}^1 a_{11}^0}{d}, & b_{24} &= \frac{a_{12}^1 a_{21}^0 - a_{22}^1 a_{11}^0}{d}, & b_{25} &= \frac{a_{15}^1 a_{21}^0 - a_{25}^1 a_{11}^0}{d}, & b_{31} &= \frac{1}{a_{66}^0}, \\
 b_{28} &= \frac{a_{18}^1 a_{21}^0 - a_{28}^1 a_{11}^0}{d}, & d &= a_{11}^0 a_{22}^0 - a_{12}^0 a_{21}^0, & b_{32} &= -\frac{2a_{66}^1}{a_{66}^0}, & b_{35} &= \frac{a_{35}^0}{a_{66}^0}, & b_{38} &= \frac{a_{38}^0}{a_{66}^0}
 \end{aligned} \tag{A1}$$

in which  $a_{ij}^{k_m}$  are described by

$$\begin{aligned}
 a_{11}^{k_1} &= \int_{-h/2}^{h/2} A_{11}(\bar{z}) z^{k_1} dz, & a_{12}^{k_1} &= \int_{-h/2}^{h/2} A_{12}(\bar{z}) z^{k_1} dz = \int_{-h/2}^{h/2} A_{21}(\bar{z}) z^{k_1} dz = a_{21}^{k_1}, \\
 a_{22}^{k_1} &= \int_{-h/2}^{h/2} A_{22}(\bar{z}) z^{k_1} dz, & a_{66}^{k_1} &= \int_{-h/2}^{h/2} A_{66}(\bar{z}) z^{k_1} dz; & k_1 &= 0, 1, 2. \\
 a_{15}^{k_2} &= \int_{-h/2}^{h/2} z^{k_2} I_1(z) A_{11}(\bar{z}) dz, & a_{18}^{k_2} &= \int_{-h/2}^{h/2} z^{k_2} I_2(z) A_{12}(\bar{z}) dz, \\
 a_{25}^{k_2} &= \int_{-h/2}^{h/2} z^{k_2} I_1(z) A_{21}(\bar{z}) dz, & a_{28}^{k_2} &= \int_{-h/2}^{h/2} z^{k_2} I_2(z) A_{22}(\bar{z}) dz, \\
 a_{35}^{k_2} &= \int_{-h/2}^{h/2} z^{k_2} I_1(z) A_{66}(\bar{z}) dz, & a_{38}^{k_2} &= \int_{-h/2}^{h/2} z^{k_2} I_2(z) A_{66}(\bar{z}) dz, & k_2 &= 0, 1.
 \end{aligned} \tag{A2}$$

### References

- Iijima, S.; Ichihashi, T. Single-shell carbon nanotubes of 1-nm diameter. *Nature* **1993**, *363*, 603–605. [\[CrossRef\]](#)
- Qian, D. Mechanics of carbon nanotubes. *Appl. Mech. Rev.* **2002**, *55*, 495–533. [\[CrossRef\]](#)
- Hirlekar, R.; Yamagar, M.; Garse, H.; Vij, M.; Kadam, V. Carbon nanotubes and its applications: A review. *Asian J. Pharm. Clin. Res.* **2009**, *2*, 17–27.
- Garg, A.; Chalak, H.D.; Belarbi, M.O.; Zenkour, A.M.; Sahoo, R. Estimation of carbon nanotubes and their applications as reinforcing composite materials-an engineering review. *Compos. Struct.* **2021**, *272*, 114234. [\[CrossRef\]](#)
- Acierno, S.; Barretta, R.; Luciano, R.; Marotti de Sciarra, F.; Russo, P. Experimental evaluations and modeling of the tensile behavior of polypropylene/single-walled carbon nanotubes fibers. *Compos. Struct.* **2017**, *174*, 12–18. [\[CrossRef\]](#)
- Tjong, S.C. Structural and mechanical properties of polymer nanocomposites. *Mater. Sci. Eng. R Rep.* **2006**, *53*, 73–197. [\[CrossRef\]](#)
- Park, C.; Wilkinson, J.; Banda, S.; Ounaies, Z.; Wise, K.E.; Sauti, G.; Lillejei, T.; Harrison, J.S. Aligned single-wall carbon nanotube polymer composites using an electric field. *J. Polym. Sci. B Polym. Phys.* **2006**, *44*, 1751–1762. [\[CrossRef\]](#)
- Chatterjee, A.; Deopura, B.L. Thermal stability of polypropylene/carbon nanofiber composite. *J. Appl. Polym. Sci.* **2006**, *100*, 3574–3578. [\[CrossRef\]](#)
- Bonnet, P.; Sireude, D.; Garnier, B.; Chauvet, O. Thermal properties and percolation in carbon nanotube-polymer composites. *Appl. Phys. Lett.* **2007**, *91*, 201910. [\[CrossRef\]](#)
- Sahoo, N.G.; Rana, S.; Cho, J.W.; Li, L.; Chan, S.H. Polymer nanocomposites based on functionalized carbon nanotubes. *Prog. Polym. Sci.* **2010**, *35*, 837–867. [\[CrossRef\]](#)
- Fantuzzi, N.; Bacciocchi, M.; Agnelli, J.; Benedetti, D. Three-phase homogenization procedure for woven fabric composites reinforced by carbon nanotubes in thermal environment. *Compos. Struct.* **2020**, *254*, 112840. [\[CrossRef\]](#)
- Zhang, X.H. Carbon nanotube/polyetheretherketone nanocomposites: Mechanical, thermal, and electrical properties. *J. Compos. Mater.* **2021**, *55*, 2115–2132. [\[CrossRef\]](#)

13. Duan, K.; He, Y.; Liao, X.; Zhang, J.; Li, L.; Li, X.; Liu, S.; Hu, Y.; Wang, X.; Lu, Y. A critical role of CNT real volume fraction on nanocomposite modulus. *Carbon* **2022**, *189*, 395–403. [[CrossRef](#)]
14. Shen, H.S. Thermal buckling and postbuckling behavior of functionally graded carbon nanotube-reinforced composite cylindrical shells. *Compos. Part B-Eng.* **2012**, *43*, 1030–1038. [[CrossRef](#)]
15. Mehar, K.; Panda, S.K. Geometrical nonlinear free vibration analysis of FG-CNT reinforced composite flat panel under uniform thermal field. *Compos. Struct.* **2016**, *143*, 336–346. [[CrossRef](#)]
16. Mirzaei, M.; Kiani, Y. Thermal buckling of temperature dependent FG-CNT reinforced composite conical shells. *Aerosp. Sci. Technol.* **2015**, *47*, 42–53. [[CrossRef](#)]
17. Shen, H.S.; Xiang, Y. Thermal buckling and postbuckling behavior of FG-GRC laminated cylindrical shells with temperature-dependent material properties. *Meccanica* **2019**, *54*, 283–297. [[CrossRef](#)]
18. Sobhy, M.; Zenkour, A.M. Thermal buckling of double-layered graphene system in humid environment. *Mater. Res. Express* **2018**, *5*, 015028. [[CrossRef](#)]
19. Mehar, K.; Panda, S.K.; Devarejan, Y.; Choubey, G. Numerical buckling analysis of graded CNT-reinforced composite sandwich shell structure under thermal loading. *Compos. Struct.* **2019**, *216*, 406–414. [[CrossRef](#)]
20. Hieu, P.T.; Tung, H.V. Thermal and thermomechanical buckling of shear deformable FG-CNTRC cylindrical shells and toroidal shell segments with tangentially restrained edges. *Arch. Appl. Mech.* **2020**, *90*, 1529–1546. [[CrossRef](#)]
21. Nam, V.H.; Trung, N.T.; Phuong, N.T.; Hung, V.T. Nonlinear torsional buckling of functionally graded carbon nanotube orthogonally reinforced composite cylindrical shells in thermal environment. *Int. J. Appl. Mech.* **2020**, *12*, 2050072. [[CrossRef](#)]
22. Hieu, P.T.; Tung, H.V. Thermal buckling and postbuckling of CNT reinforced composite cylindrical shell surrounded by an elastic medium with tangentially restrained edges. *J. Thermoplast. Compos. Mater.* **2021**, *34*, 861–883. [[CrossRef](#)]
23. Sofiyev, A.; Bayramov, R.P.; Heydarov, S.H. The forced vibration of infinitely long cylinders reinforced by carbon nanotubes subjected to combined internal and ring-shaped compressive pressures. *Math. Meth. Appl. Sci.* **2020**, 1–12. [[CrossRef](#)]
24. Mota, A.F.; Loja, M.A.R.; Barbosa, J.I.; Rodrigues, J.A. Porous functionally graded plates: An assessment of the influence of shear correction factor on static behavior. *Math. Comput. Appl.* **2020**, *25*, 25. [[CrossRef](#)]
25. Turuelo, C.G.; Breitkopf, C. Simple algebraic expressions for the prediction and control of high-temperature annealed structures by linear perturbation analysis. *Math. Comput. Appl.* **2021**, *26*, 43.
26. Monaco, G.T.; Fantuzzi, N.; Fabbrocino, F.; Luciano, R. Trigonometric solution for the bending analysis of magneto-electro-elastic strain gradient nonlocal nanoplates in hygro-thermal environment. *Mathematics* **2021**, *9*, 567. [[CrossRef](#)]
27. Monaco, G.T.; Fantuzzi, N.; Fabbrocino, F.; Luciano, R. Critical temperatures for vibrations and buckling of magneto-electro-elastic nonlocal strain gradient plates. *Nanomaterials* **2021**, *11*, 87. [[CrossRef](#)] [[PubMed](#)]
28. Trang, L.T.N.; Tung, H.V. Thermoelastic stability of thin CNT-reinforced composite cylindrical panels with elastically restrained edges under nonuniform in-plane temperature distribution. *J. Thermoplast. Compos. Mater.* **2021**. [[CrossRef](#)]
29. Chakraborty, S.; Dey, T.; Kumar, R. Instability characteristics of damped CNT reinforced laminated shell panels subjected to in-plane excitations and thermal loading. *Structures* **2021**, *34*, 2936–2949. [[CrossRef](#)]
30. Babaei, H. Thermoelastic buckling and post-buckling behavior of temperature-dependent nanocomposite pipes reinforced with CNTs. *Eur. Phys. J. Plus* **2021**, *136*, 1093. [[CrossRef](#)]
31. Babaei, H. On frequency response of FG-CNT reinforced composite pipes in thermally pre/post buckled configurations. *Compos. Struct.* **2021**, *276*, 114467. [[CrossRef](#)]
32. Baccocchi, M.; Fantuzzi, N.; Ferreira, A.J.M. Static finite element analysis of thin laminated strain gradient nanoplates in hygro-thermal environment. *Contin. Mech. Thermodyn.* **2021**, *33*, 969–992. [[CrossRef](#)]
33. Moita, J.S.; Araújo, A.L.; Correia, V.F.; Soares, C.M.M. Mechanical and thermal buckling of functionally graded axisymmetric shells. *Compos. Struct.* **2021**, *261*, 113318. [[CrossRef](#)]
34. Avey, M.; Fantuzzi, N.; Sofiyev, A.H. Thermoelastic stability of CNT patterned conical shells under thermal loading in the framework of shear deformation theory. *Mech. Adv. Mater. Struct.* **2022**; *in press*. [[CrossRef](#)]
35. Avey, M.; Sofiyev, A.H.; Kuruoglu, N. Influence of elastic foundations and thermal environments on the thermoelastic buckling of nanocomposite truncated conical shells. *Acta Mech.* **2022**, *233*, 685–700. [[CrossRef](#)]
36. Allam, M.N.M.; Radwan, A.F.; Sobhy, M. Hygrothermal deformation of spinning FG graphene sandwich cylindrical shells having an auxetic core. *Eng. Struct.* **2022**, *251*, 113433. [[CrossRef](#)]
37. Ambartsumyan, S.A. *General Theory of Anisotropic Shells*; Nauka: Moscow, Russia, 1974.
38. Reddy, J.N. *Mechanics of Laminated Composite Plates and Shells*; CRC Press: Boca Raton, FL, USA, 2004.
39. Eslami, M.R. *Buckling and Postbuckling of Beams, Plates, and Shells: Buckling of Conical Shells*; Springer: Cham, Switzerland, 2018.
40. Sofiyev, A.H. Thermo elastic stability of functionally graded truncated conical shells. *Compos. Struct.* **2007**, *77*, 56–65. [[CrossRef](#)]
41. Shen, H.S. Postbuckling of nanotube-reinforced composite cylindrical shells in thermal environments, Part I: Axially-loaded shells. *Compos. Struct.* **2011**, *93*, 2096–2108. [[CrossRef](#)]